On the Roles of Substrate Binding and Hinge Unfolding in Conformational Changes of Adenylate Kinase

Jason B. Brokaw[†] and Jhih-Wei Chu[‡*]
[†]Department of Chemistry and [‡]Department of Chemical and Biomolecular Engineering, University of California, Berkeley, California

ABSTRACT We characterized the conformational change of adenylate kinase (AK) between open and closed forms by conducting five all-atom molecular-dynamics simulations, each of 100 ns duration. Different initial structures and substrate binding configurations were used to probe the pathways of AK conformational change in explicit solvent, and no bias potential was applied. A complete closed-to-open and a partial open-to-closed transition were observed, demonstrating the direct impact of substrate-mediated interactions on shifting protein conformation. The sampled configurations suggest two possible pathways for connecting the open and closed structures of AK, affirming the prediction made based on available x-ray structures and earlier works of coarse-grained modeling. The trajectories of the all-atom molecular-dynamics simulations revealed the complexity of protein dynamics and the coupling between different domains during conformational change. Calculations of solvent density and density fluctuations surrounding AK did not show prominent variation during the transition between closed and open forms. Finally, we characterized the effects of local unfolding of an important hinge near Pro^{177} on the closed-to-open transition of AK and identified a novel mechanism by which hinge unfolding modulates protein conformational change. The local unfolding of Pro^{177} hinge induces alternative tertiary contacts that stabilize the closed structure and prevent the opening transition.

INTRODUCTION

Conformational change is an essential mechanism by which the biological functions of protein molecules are regulated and coordinated in living organisms (1–3). Characterizing the pathways of protein conformational change can therefore shed light on how to regulate biological processes at the molecular level (2,4–6). The end states of a conformational change are often visualized by the x-ray structures of a protein at different states, such as substrate-bound (SB) versus apo. It has often been observed that regions distal to the substrate-binding site are also affected. The connection between local changes in molecular interactions and global changes in protein conformation is still a puzzle (1,2,7). The classic lock-and-key (8) and induced-fit (9) theories have been updated with conformational selection or population shift mechanisms, which suggest that substrate binding shifts the equilibrium between different conformational states that preexist even without the substrate (10–17). It is also established that protein motions span a wide range of timescales and length scales (18), and different modes of motion may exhibit various correlations with protein function (14,15). However, causative relationships are much more difficult to establish and require high-resolution methods. Therefore, molecular-dynamics (MD) simulations are often employed to provide complementary information (19,20).

An intrinsic structural transition of proteins that would couple with conformational change is local unfolding (21–25), the tendency of which depends on the protein sequence as well as the solvation environment (26–28). Local unfolding has a direct impact on protein function by affecting structures and flexibility (21–30). The introduction of locally unfolded structures is also used as a strategy to generate an approximate ensemble of protein structures for modeling protein cooperativity and allostery (29,31). It has also been proposed that mechanical strains produced by protein motions induce local unfolding to facilitate the functional conformational changes of proteins (32–34).

To study the effects of substrate binding and local unfolding on protein conformational changes, we analyzed *Escherichia coli* adenylate kinase (AK) by means of all-atom MD simulations (35,36). AK catalyzes the phosphoryl transfer between two ADP molecules to yield ATP and AMP to regulate cellular energy homeostasis (37). The conformational changes of AK have been shown to exhibit a strong correlation with enzyme activity (34,38–41). Kinetic experiments (16,17,35,42,43) suggested conformational change as a rate-limiting step for catalysis. Recent single-molecule Förster resonance energy transfer experiments (41) affirmed that the conformational change from a closed to an open conformation after the phosphoryl transfer is the rate-limiting step of the reverse ATP-producing reaction of AK.

X-ray structures of AK in SB (36,44) and apo (35) forms show that both the LID and NMP_{bind} travel a long distance (>9 Å) to transit from the open (substrate-free) to the closed (SB) structure (Fig. 1 and Fig. S1 in the Supporting Material). Inspection of both structures suggests that the closed-to-open transition facilitates product release and substrate binding to complete a catalytic cycle. Single-molecule Förster resonance energy transfer studies provide solid evidence that the transition between the closed and

Submitted May 5, 2010, and accepted for publication September 21, 2010.

*Correspondence: jwchu@berkeley.edu

Editor: Gerhard Hummer.

0006-3495/10/11/3420/10 $2.00

doi: 10.1016/j.bpj.2010.09.040

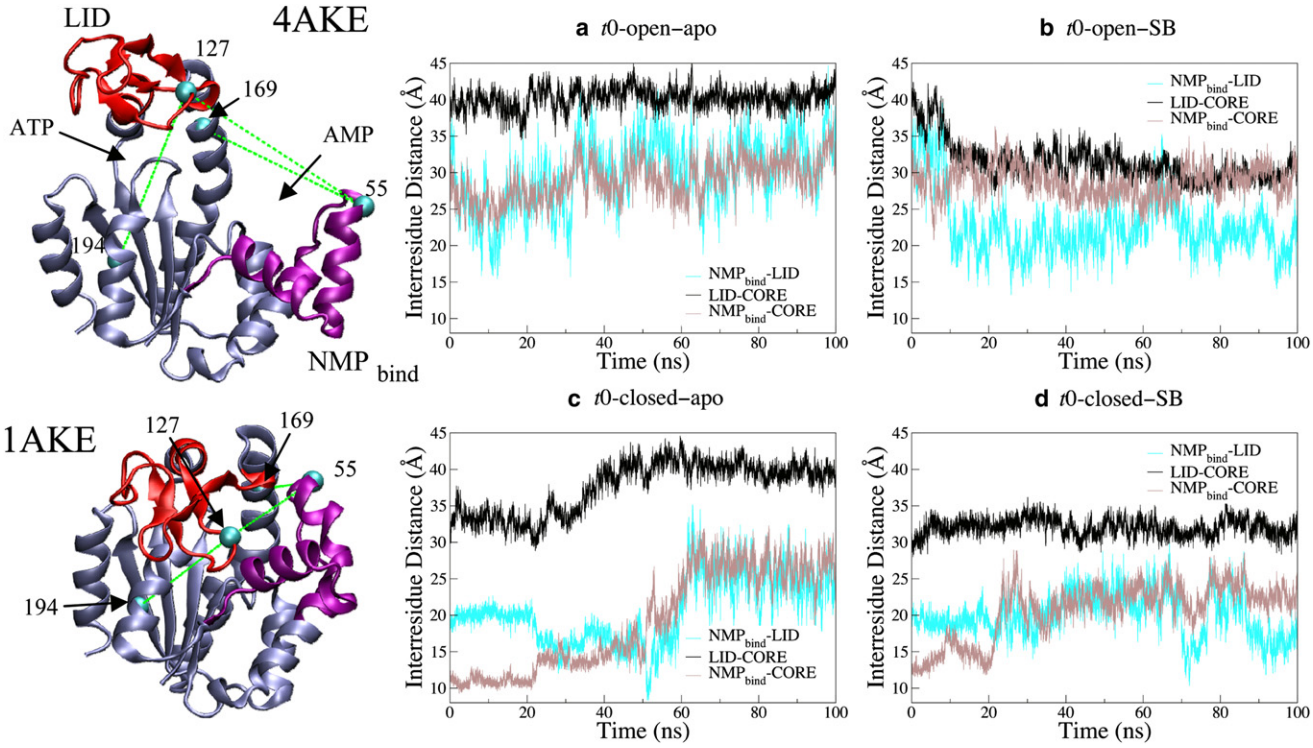

FIGURE 1 Interresidue distances tracking the open (4AKE) and closed (1AKE) conformations of AK (*left*). NMP_{bind}-LID (*cyan/light*) is the C_α-C_α distance between residues 55 (NMP_{bind}) and 127 (LID). LID-CORE (*black*) is the C_α-C_α distance between residues 127 (LID) and 194 (CORE). NMP_{bind}-CORE (*brown/dark*) is the C_α-C_α distance between residues 55 (NMP_{bind}) and 169 (CORE). Results from the (*a*) *t*0-open–apo simulation, (*b*) *t*0-open–SB simulation, (*c*) *t*0-closed–apo simulation, and (*d*) *t*0-closed–SB simulation are shown. See text for the definitions of all-atom MD simulations.

open states of AK undergoes dynamic equilibrium even without the presence of substrate, and that the presence of substrate changes the populations of open and closed forms and transition rates (41). NMR studies show that the backbone flexibility of AK is reduced in the presence of inhibitor molecule AP_5A (45,46). In particular, the motions of hinge regions have been shown to have a high correlation with substrate binding and enzyme activity (13,47,48).

The strong correlation between the conformational dynamics and enzyme activity makes AK a popular system for modeling the functional roles of protein conformational changes (39,40,47,49–54). Results from all-atom MD simulations indicate that the low-frequency harmonic modes around the open form involve directions that correspond to the open-to-closed transition (47,50,54). Typically employed order parameters for describing the transition between closed and open AK include distances between residues in different domains (39), angles between domains (55), and the relative root mean-squared distances (RMSDs) between the open and closed structures (40). Using the distance between centers of mass of Ala^{55} and Val^{169}, Lou and Cukier (39) found that NMP_{bind} closing in apo AK has a decreasing potential of mean force, with a change of –2.0 kcal/mol. Using the relative RMSDs between open and closed structures, Arora and Brooks (40) found that the open-to-closed transition in SB AK has a decreasing free-energy profile, with a change of –12.5 kcal/mol, and the free-energy profile along the relative RMSD coordinate is a strong function of substrate binding.

Because AK closing requires the LID and NMP_{bind} to move toward the CORE, it could proceed through multiple pathways, such as LID-closes-first or NMP_{bind}-closes-first mechanisms. The x-ray structures of mutant yeast and bovine AK also suggest that LID-closed/NMP_{bind}-open and LID-open/NMP_{bind}-closed structures are accessible states (56,57). The presence of both LID-closes-first and NMP_{bind}-closes-first mechanisms has also been predicted by molecular modeling. In particular, a double-well network model that interpolates the internal coordinates of two coarse-grained (CG) elastic network models resolved both mechanisms (58). Interpolating Gō model representations led to a similar result (59,60). However, because the mechanisms deduced by CG modeling depend on the scheme used to interpolate protein topology (58), validation with finer-grained atomic force fields is required.

In this work, we analyze the open-to-closed as well as closed-to-open transitions of AK via extensive all-atom MD simulations in explicit solvent with a focus on elucidating the effects of substrate binding and hinge unfolding. In particular, we characterize 1), the sequential order of the LID and NMP_{bind} along transition pathways; 2), the effects of local unfolding of the hinge around Pro^{177} on the closed-to-open

transition; and 3), the changes in the solvation environment of AK during the closing and opening transitions. All-atom MD simulations were performed in explicit water for 100 ns in each of the sampled trajectories.

We found that the closed-to-open transition in apo AK follows a LID-opens-first route (NMP_{bind}-closes-first in the reverse transition). Our results also indicate that the open-to-closed transition in SB AK is likely to follow a LID-closes-first mechanism, since in the presence of substrate the LID quickly closed from the open structure, whereas the NMP_{bind} remained open. Together, the results from our all-atom MD simulations support the predictions made by the double-well network model (58) and other CG models (59,60) that two alternative pathways can be found to connect open and closed AK.

During the observed closed-to-open and open-to-closed transitions in all-atom MD, the hinge region around Pro^{177} appears to play important roles in providing structural support. To test this hypothesis, we locally unfolded the Pro^{177} hinge and analyzed its impact on the closed-to-open transition in apo AK. Local unfolding of the Pro^{177} hinge perturbed the orientation between nearby helices and induced alternative interdomain interactions. As a result, the opening transition did not occur in the simulation with an unfolded Pro^{177} hinge, in contrast to the case in which the Pro^{177} hinge was folded.

Furthermore, we quantified the level of desolvation that accompanies the closing of the LID and NMP_{bind}, and at the active site. The results indicate that substrate binding and closing exclude water primarily at the active site without causing a significant change in the other parts of AK. There is no pronounced change in water density near AK, and large changes in density fluctuations are not observed during structural transitions. The open-to-closed transition of AK does not involve burying an extended hydrophobic patch, consistent with computational and theoretical studies on the hydration of model surfaces (61–64).

In the following, we first describe in detail the different sets of MD simulations that were performed in this work. We then describe the results of the conformational dynamics of AK. Finally, we finish with concluding remarks.

RESULTS AND DISCUSSION

Substrate-binding induced transitions between closed and open AK

The results presented in this section include a total of four 100 ns all-atom MD trajectories performed at 300 K and 1 atm using the CHARMM force field with CMAP terms (65,66). In the simulation started from the open form of AK without ATP or AMP, termed the *t*0-open–apo simulation, initial coordinates were taken from Protein Data Bank (PDB) ID 4AKE (35). In the simulation started from the open structure in the presence of ATP and AMP (which are docked to the active site according to the closed x-ray structure PDB ID 2ECK), the *t*0-open–SB simulation, initial coordinates were also taken from PDB ID 4AKE. In the simulation starting from the closed structure without ATP or AMP (*t*0-closed–apo), initial coordinates were taken from PDB ID 1AKE (36). In the simulation starting from the closed structure with ATP and AMP (*t*0-closed–SB), initial coordinates were taken from PDB ID 2ECK (RMSD to 1AKE = 0.3 Å (44)). In the SB simulations, the initial coordinates of ATP and AMP were determined based on the structures of PDB ID 2ECK (44), which contains the coordinates of a substrate analog. The backbone atoms of 2ECK were oriented against the reference x-ray structure to determine the coordinates of the substrate. In a similar manner, the initial coordinates of the Mg^{2+} ion were determined using PDB ID 2CDN (*Mycobacterium tuberculosis* AK) (67), which resolved the metal ion at AK active site. In preparing the initial structure of the *t*0-open–SB simulation, only active site atoms were used in the structural orientation, and ATP+Mg^{2+} and AMP were placed in each of their binding sites separately.

From the four trajectories, the interresidue distances tracking the opening and closing of the LID and NMP_{bind} were calculated every 10 ps, as shown in Fig. 1. The RMSDs to 1AKE and 4AKE crystal structures from these simulations are presented in Fig. S2 for comparison. The NMP_{bind}-LID distance is estimated by the C_α-C_α distance between residues 55 (NMP_{bind}) and 127 (CORE), the LID-CORE distance is estimated by the C_α-C_α distance between residues 127 (CORE) and 194 (LID) (41), and the NMP_{bind}-CORE distance is estimated by the C_α-C_α distance between residues 55 (NMP_{bind}) and 169 (CORE). It can be seen that in the *t*0-open–apo simulation, AK remained open during the course of 100 ns (Fig. 1 *a*), and all three distances fluctuated around the values corresponding to the open form.

In the *t*0-open–SB simulation, the LID closed as a result of substrate-mediated interactions, but NMP_{bind} remained open. The LID-CORE and NMP_{bind}-LID distances decreased by 10 and 15 Å, respectively. LID closing started at ~5 ns and finished at ~15 ns, after which the LID remained closed. When the LID closed, the distances between positively charged residues in the CORE and LID, such as Lys^{13} (CORE) and Arg^{123} (LID), shrank by forming contacts with the phosphates of ATP. These electrostatic interactions were also observed in the x-ray structure of closed AK (36,44). The NMP_{bind}-CORE distance, on the other hand, fluctuated around the value in the open initial structure (Fig. 1 *b*) even though AMP was placed in the binding pocket (a snapshot is shown in Fig. S1, *top center*). In the x-ray structure of closed AK, Arg^{156} at the CORE-LID boundary and Arg^{88} in NMP_{bind} form contacts with the phosphate group of AMP, and Lys^{57} (LID) and Glu^{170} (NMP_{bind}) are also in contact (36,44). Although the adenosine group of AMP stayed in the hydrophobic pocket of NMP_{bind} during the course of the 100 ns *t*0-open–SB

simulation, the aforementioned electrostatic interactions did not form, leading to a LID-closed–NMP_{bind}-open structure. The transition observed in the *t*0-open–SB simulation thus corresponds to a LID-closes-first mechanism.

In the closed structure of AK, NMP_{bind} differs from the open form with an overstretched α3 and altered orientations between the α2, α3, and α4 helixes, which form the hydrophobic core that binds the adenosine group of AMP (35,36,44). Based on these structural differences, it has been suggested that strain-induced local unfolding might be involved in closing NMP_{bind} (32,34). This would be consistent with the results of a recent simulation work that used an atomic force field with implicit solvent and bias potentials (55). In the 100 ns *t*0-open–SB simulation of this work, neither α3 local unfolding nor NMP_{bind} closing occurred, and this correlation did not contradict the theory of local-unfolding–induced NMP_{bind} closing.

In the *t*0-closed–apo simulation, both LID and NMP_{bind} opened after ATP and AMP were removed from the binding pocket. Opening started around 20 ns with the LID, and NMP_{bind} followed at ~50–60 ns (Fig. 1 *c*). AK became fully open at ~60 ns. Compared to the initial structure, NMP_{bind}-LID, LID-CORE, and NMP_{bind}-CORE distances increased during the course of the *t*0-closed–apo simulation by 5, 10, and 15 Å, respectively (Fig. 1*c*). Within the first 5 ns during the *t*0-closed–apo simulation, while the LID still remained closed, the dislocated bend around the Pro^{177} hinge observed in the closed x-ray structure relaxed to an intact helix and remained so throughout the simulation (Fig. S3). However, this structural change did not lead to immediate LID opening (which started 15 ns later) or a noticeable change in the end-to-end distance of the α7-α8 helix that contains Pro^{177} (the C_α-C_α distance between residues 161 and 188 remained ~40 Å). Straightening of the dislocated bend around the Pro^{177} hinge was also observed in the *t*0-closed–SB simulation, in which the LID remained closed (Fig. 1 *d*). In the *t*0-open–SB simulation discussed above, in which LID closed due to ATP-mediated interactions (Fig. 1 *b*), the dislocated bend observed in the x-ray structure of closed AK did not form. Therefore, a dislocated bend around the Pro^{177} hinge is not required for LID closing.

For NMP_{bind} opening in the *t*0-closed–apo simulation, in addition to increased distances between positively charged residues such as Arg^{156} (CORE) and Arg^{88} (NMP_{bind}), relaxation of the overstretched α3 observed in the closed crystal structure (residues 44–56; Fig. S3) (35,36,44) also occurred. The α3 relaxation shortly preceded NMP_{bind} opening and affected four to five backbone hydrogen bonds, resulting in a ~20 kcal/mol reduction of backbone hydrogen-bonding energy (Fig. S4). Relaxation of the overstretched α3 was also observed in the *t*0-closed–SB simulation, and NMP_{bind} opened about halfway as compared to the open crystal structure (Fig. 1). This observation suggests that overstretching α3 is likely involved in NMP_{bind} closing, and cracking (strain-induced local unfolding) may facilitate of NMP_{bind} closing (32,34,55). The observation in the *t*0-open–SB simulation that both α3 overstretching and NMP_{bind} closing did not occur (Fig. 1 *b*) does not contradict this theory.

In addition to overstretching α3, the x-ray structures of closed AK also show altered orientations between α2, α3, and α4 helixes as compared to the open form (36). The α2, α3, and α4 helixes form the hydrophobic core of NMP_{bind} that binds the adenosine group of AMP. The charged residues of NMP_{bind} mostly reside at the surfaces that interface with LID, CORE, and the phosphate group of AMP. Therefore, the opening and closing of NMP_{bind} involve a balance between electrostatic interactions, backbone hydrogen bonding in secondary structures, and hydrophobic interactions.

In the *t*0-closed–apo simulation, the opening transition started at ~20 ns and took ~40 ns to finish (Fig. 1 *c*). The opening involved two distinct steps: LID opened first (20–40 ns), followed by NMP_{bind} (40–60 ns). LID opening also led to changes in NMP_{bind}-CORE and NMP_{bind}-LID distances in opposite directions (Fig. 1 *c*), highlighting the coupled dynamics between these domains. NMP_{bind} started to open right after the completion of LID opening (Fig. 1 *c*). The reverse of this path (i.e., closing) corresponds to a NMP_{bind}-closes-first mechanism, opposite to the LID-closes-first partial transition observed in the *t*0-open–SB simulation (Fig. 1 *b*). Both the opening and partial closing transitions of AK started with the more extended and flexible LID, as predicted via topology-based CG models (34,58–60).

The all-atom MD simulations presented above provide direct evidence that the structural flexibility, substrate-mediated interactions, and mechanical properties of local structures (Pro^{177} hinge and the α3 helix) are all important factors in determining the directionality and pathways of protein conformational change. The AK structures sampled in *t*0-open–apo (*red*), *t*0-open–SB (*blue*), *t*0-closed–apo (*green*), and *t*0-closed–SB (*black*) simulations are projected onto a two-dimensional surface parameterized by LID-CORE and NMP_{bind}-CORE distances in Fig. 2. In the *t*0-open-apo simulation (Fig. 2, *red*), both LID-CORE and NMP_{bind}-CORE distances remained open. In the *t*0-open–SB simulation (Fig. 2, *blue*), ATP-mediated interactions led to LID closing. Conversely, NMP_{bind} remained open in the presence of AMP, but without an overstretched α3. Similarly, relaxing the overstretched α3 in the *t*0-closed–SB simulation (*black*) led to the partial opening of NMP_{bind}.

In both the *t*0-open–SB and *t*0-closed–SB simulations (Fig. 2, *black and blue*), the LID closed from open or remained closed due to substrate-mediated interactions. Therefore, a LID-closed–NMP_{bind}-open state may be an intermediate on a LID-closes-first pathway mediated by substrate binding. The distributions of NMP_{bind}-CORE distance in both simulations clearly overlap (Fig. 2). NMP_{bind} closing, however, was not observed in the *t*0-open–SB

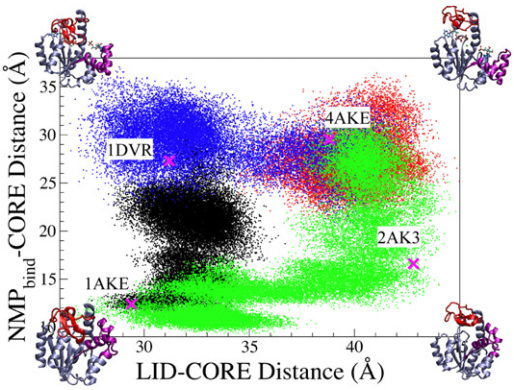

FIGURE 2 Distribution of LID-CORE (*x* axis) and NMP$_{bind}$-CORE (*y* axis) distances observed in four 100 ns trajectories of all-atom MD simulations: (*green/bottom and right*) *t*0-closed–apo, (*red/top right*) *t*0-open–apo, (*blue/top left and top right*) *t*0-open–SB, and (*black*) *t*0-closed–SB. See text for the definition of all-atom MD simulations. The definitions of LID-CORE and NMP$_{bind}$-CORE distances are described in Fig. 1. The corresponding distances and PDB codes of several crystal structures of AK and AK variants are shown.

simulation (Fig. 1 *b*). At the end of the *t*0-open–SB simulation, Fig. 1 *b* shows an NMP$_{bind}$-CORE distance of ~30 Å, which is distinct from the value of 22 Å in the *t*0-closed–SB simulation. The smallest RMSD between configurations sampled in the last 20 ns of both simulations is 1.9 Å.

By performing all-atom MD simulations of AK in explicit solvent without applying any bias potential, we were able to show that open and closed AKs are likely to be connected by at least two distinct pathways (Fig. 2), as predicted previously by CG modeling (58–60). These results also establish that introducing and removing protein-substrate interactions alone can drive LID closing and the opening of LID and NMP$_{bind}$. The dual-path character of AK conformational change was also inferred from previous structural analyses via x-ray crystallography (56,57). LID-CORE and NMP$_{bind}$-CORE distances that correspond to LID-closed-NMP$_{bind}$-open (1DVR) and LID-open-NMP$_{bind}$-closed (2AK3) crystal structures are also shown in Fig. 2 for comparison. The all-atom MD simulations sampled the distances observed in both structures. An analysis of the C_α root mean-square fluctuation (RMSF) as a function of AK conformation can be found in Fig. S5 for comparison.

Local unfolding of the Pro^{177} hinge affected the closed-to-open transition of AK and induced alternative interdomain interactions

In the *t*0-closed–apo and *t*0-closed–SB simulations, the dislocated bend of the Pro^{177} hinge in the closed structure (36) relaxed quickly. The Pro^{177} hinge is located in a helix-X-helix motif of AK (residues 161–189) that connects LID and CORE (68); residues 161–175 are the α7 helix, and residues 177–189 are the α8 helix (35,36) (Fig. S3). Pro^{177} is situated in the middle of this motif and caps the end of α8 (Fig. S3). Therefore, the helix-X-helix motif can sustain small perturbations, such as the dislocated bend to maintain an adequate structural framework for AK to adapt to substrate-mediated interactions by opening or closing the LID. Although the *t*0-open–SB simulation shows that neither a dislocated bend nor local unfolding is required to accommodate LID closing, local unfolding as a naturally occurring structural change in the presence of thermal energy may still affect the conformational change of AK by altering the structural framework of the helix-X-helix motif. This hypothesis is also motivated by the facts that proline is a disruptor of α-helixes and Pro^{177} is a highly conserved residue among AKs that contain a bulky LID (54). To probe the impact of the Pro^{177} hinge on the closed-to-open transition of AK, we performed all-atom MD simulations using different initial structures.

First, we unfolded the helical structure between residues 169 and 175 in the closed form using a harmonic potential. Second, we performed an 11 ns simulation in the presence of a restraint potential to keep the hinge region unfolded with another restraint potential to other residues so that their structures would be maintained close to the closed x-ray structure. After this step, the simulation was continued for 100 ns without applying any restraint potential. The starting structure of this *t*0-closed–apo-Pro^{177}-UF simulation is shown in the top left of Fig. 3.

Contrary to the *t*0-closed–apo simulation, in which the LID opened, the LID-CORE distance in the *t*0-closed–apo-Pro^{177}-UF simulation fluctuated around the value of the x-ray structure of closed AK (Fig. 3), i.e., the LID remained closed. This result shows that local unfolding of the Pro^{177} hinge altered the conformational response of AK after removing the bound substrates. Instead of LID opening, the binding pocket expanded to compensate for

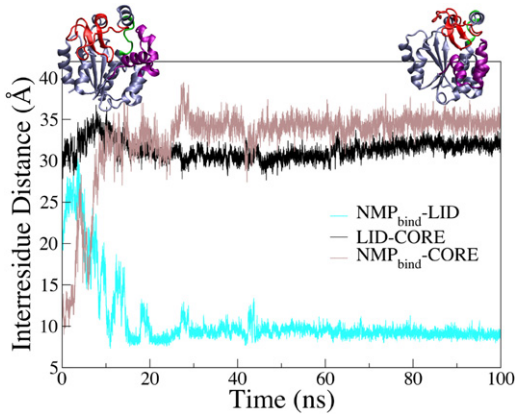

FIGURE 3 Time evolution of the interresidue distances of AK during the *t*0-closed–apo-Pro^{177}-UF simulation. NMP$_{bind}$-LID (*cyan/light*), LID-CORE (*black*), and NMP$_{bind}$-CORE (*brown/dark*) distances are shown. Definitions of the interresidue distances are given in Fig. 1. Top left is the starting structure and top right is the ending structure of AK in the *t*0-closed–apo-Pro^{177}-UF simulation.

the absence of protein-substrate interactions. For example, the distance between the terminal guanidinium nitrogens of Arg^{88} and Arg^{167} (both CORE) increased from 8 to 14 Å in both *t*0-closed–apo and *t*0-closed–apo-Pro^{177}-UF simulations. This result was accomplished by LID opening in the former, and by formation of a more expanded binding pocket with a closed LID in the latter. This result provides direct evidence that local unfolding of the Pro^{177} hinge can impact the closed-to-open transition of AK. Using a different force field to examine the unfolding of Pro^{177} hinge, we made a similar observation. Discussion of this simulation is provided in the Supporting Material and Fig. S6.

The structures sampled in the *t*0-closed–apo-Pro^{177}-UF simulation differ from those sampled in the simulations mentioned above, in each of which the Pro^{177} hinge had an intact helical structure. After the Pro^{177} hinge was unfolded, the more extended structure induced alternative interdomain interactions. As an example, in the *t*0-closed–apo-Pro^{177}-UF simulation, Arg^{36} (NMP_{bind}) formed a hydrogen bond with Ser^{129} in LID (Fig. S7, *right*) instead of interacting with Asp^{158} as in the *t*0-closed–apo simulation (Fig. S7, *left*). The Arg^{36}-Ser^{129} hydrogen bond is specific to the case in which the Pro^{177} hinge was unfolded; it was not observed in any of the simulations in which the Pro^{177} hinge was in the helical structure. Other examples of new contacts (residues with heavy atoms within 4 Å of each other) that formed in the *t*0-closed–apo-Pro^{177}-UF simulation but not in the closed (1AKE) or open (4AKE) crystal structures are shown in Table 1. These contacts are divided into three main categories of rearrangements: 1), in the substrate-binding pockets; 2), between LID and NMP_{bind}; and 3), in the Pro^{177} hinge itself. Therefore, hinge unfolding shifts apo AK conformations into a different closed structure. In addition, the alternative contacts allowed by the unfolding of the Pro^{177} hinge result in a significant difference in the distribution of residue RMSF (Fig. S8, *top*). Together with the simulations shown in Figs. 2 and 3, the results show that AK conformational changes are a strong function of substrate binding, defects of secondary structures, hinge unfolding, and alternative tertiary contacts.

The involvement of many degrees of freedom complicates the characterization of protein conformational change.

TABLE 1 New contacts formed in the *t*0-closed–apo-Pro^{177}-UF simulation

Substrate-binding site	LID-NMP	Pro^{177} hinge
PRO^{9}–ARG^{119}	ARG^{36}–SER^{129}*	ARG^{167}–THR^{175}*
GLY^{10}–PHE^{137}	MET^{53}–PRO^{128}	VAL^{117}–LEU^{168}
ARG^{88}–ASP^{158}*	LEU^{58}–VAL^{125}	LYS^{166}–MET^{174}
	LEU^{58}–ARG^{156}	

Statistics are taken from the final 20 ns of the simulation. The listed contacts are not observed in the open and closed x-ray structures of AK, in which the Pro^{177} hinge assumes a helical structure. Contacts are defined as residues containing heavy atoms within 4 Å of each other. *Polar or charged electrostatic contact.

In addition to LID-CORE and NMP_{bind}-CORE distances, as shown in Fig. 2, LID-NMP_{bind} distance is also important for specifying AK conformation. For example, using the NMP_{bind}-CORE distance (C_α-C_α distance between residues 55 [NMP_{bind}] and 169 [CORE]), the final structure of the *t*0-closed–apo-Pro^{177}-UF simulation can be considered as NMP_{bind}-open; a transition from 12.2 to 32.7 Å occurred. However, the NMP_{bind}-LID distance (C_α-C_α distance between residues 55 and 127) remained small (11 ± 4 Å). Therefore, if the NMP_{bind}-LID distance is used as an order parameter, the final structure of the *t*0-closed–apo-Pro^{177}-UF simulation would be considered NMP_{bind} closed. Thus, it is difficult to assign the open and closed states of NMP_{bind} with a single interdomain distance.

The results of the all-atom MD simulations can also be compared with experimental observations. Single-molecule experiments using LID-CORE (41) or NMP_{bind}-LID (47) distances indicate that even under the substrate-free conditions, the closed structures of AK are significantly populated. All-atom MD simulations indicate that each of the order parameters used in the experiments provides only a partial description of AK conformation (Fig. 1), and that the open and closed structures defined by either order parameter may not be consistent with the result of using the other. Using LID-CORE distance as an order parameter, Hanson et al. (41) showed that the closed state is more populated than the open state in the substrate-free condition. As shown by all-atom MD simulations, local unfolding of the Pro^{177} hinge can lead to alternative tertiary contacts that keep the LID in a closed form. Therefore, configurations with an unfolded Pro^{177} hinge are also likely to be significantly populated. The high backbone flexibility of residues around the Pro^{177} hinge as measured by NMR (around hinge 8 in Henzler-Wildman et al. (54)) supports this hypothesis. Therefore, the simulation results presented in this work should prompt further experimental characterizations of the structural distribution of the Pro^{177} hinge.

The results of all-atom MD simulations illustrate many instances in which the mechanical properties of protein structures are coupled to AK conformational changes. First, the sequential order of conformational change is correlated with the relative flexibilities of different domains. The LID in open AK is more extended and flexible, and both the opening and closing transitions of AK started with the LID (Fig. 2). Second, protein-substrate interactions can distort secondary structures, and the resulting strain can drive conformational change. The overstretched α3 helix led to the partial opening and opening of NMP_{bind} in the *t*0-closed–SB and *t*0-closed–apo simulations, respectively. Third, local secondary structures, such as those around the Pro^{177} hinge, can change the responses of protein conformation to substrate-mediated interactions. Formation of alternative tertiary contacts was observed to maintain a LID-closed conformation after the Pro^{177} hinge was unfolded. Therefore, the flexibility and mechanical

properties of the protein structure are essential parameters for describing conformational changes.

Solvation structures surrounding AK during structural transitions

Another important consideration is whether protein conformational changes are associated with concomitant changes in the solvation environment. To address this question, we calculated the average water coordination number (WCN), i.e., the number of water molecules within 5.0 Å of any atom in AK (Fig. 4, *top*). The results indicate that the WCN is a strong function of protein conformation, but this dependence is highly correlated with the available solvation volume around the protein (Fig. 4, *bottom*). We estimated the solvation volumes shown in Fig. 4 by using the difference between the volume within 5.0 Å of any protein atom and within 1.7 Å of any protein atom. Using this estimation of solvation volume and a 5.0 Å cutoff for WCN, we were able to demonstrate a relatively constant water number density of 0.0337 ± 0.0006 $Å^{-3}$ near AK. Therefore, the variation of WCN during the structural transition of AK is mostly due to changes in the available solvation volume as the protein changes its structure.

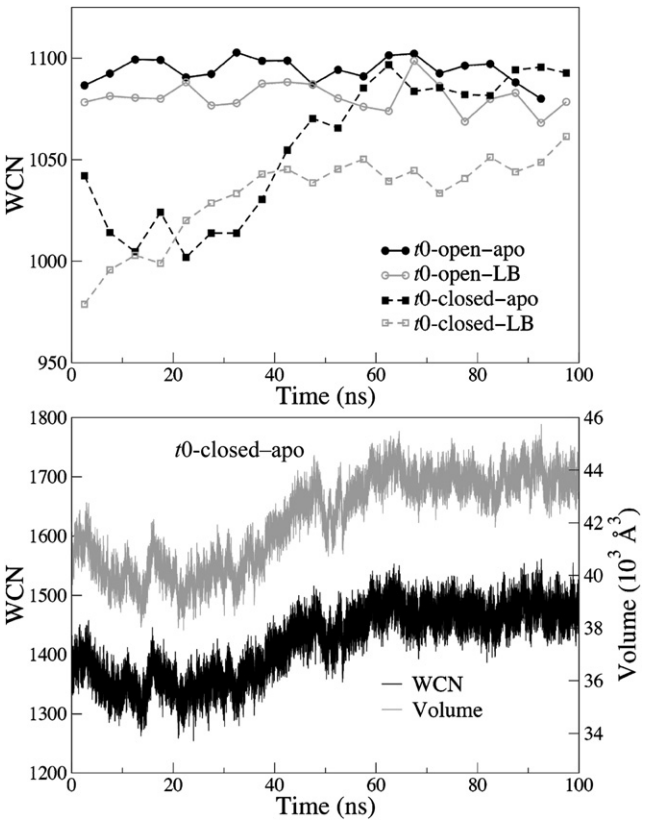

FIGURE 4 Top: Time evolution of the block-averaged (5 ns) WCN of AK in four 100 ns all-atom MD simulations. Bottom: Time evolution of the WCN and solvation volume of AK in the *t*0-closed-apo simulation.

WCNs around the different domains of AK are shown in Fig. S9.

In addition to solvent density, density fluctuations can also be affected by protein structure, reflecting solvent-mediated driving forces such as hydrophobic interactions for conformational changes (62,69–73). To compute the fluctuations of water density around AK, we sorted the structures sampled in the all-atom MD simulations according to solvation volume (bin size = 100 $Å^3$). The isothermal compressibility of water in each volume bin was then determined for different simulations. The value observed in all simulations, computed as $(\langle WCN^2\rangle - \langle WCN\rangle^2)/\langle WCN\rangle$, 0.128 ± 0.005 (see Fig. S10), is comparable to those obtained in other studies (72). We observed no discernible dependence of water compressibility on AK conformation. Since the conformational changes of AK do not involve burying or exposing an extended hydrophobic patch, this result is consistent with theoretical and computational studies on the hydration of model surfaces (61–64).

To examine whether specific protein-water hydrogen bonds undergo significant changes during AK conformational changes, we calculated the average number of hydrogen bonds that each amino acid formed with water in every 1 ns window during each of the four 100 ns trajectories shown in Fig. 2. The results are shown in Fig. S11. The changes in the number of residue-water hydrogen bonds between time windows were also calculated and are shown in Fig. S12. We did not observe any prominent variation of residue-water hydrogen bonds during AK conformational changes. However, we did identify subtle differences between the SB and apo simulations. Residues that coordinated with the substrate displayed distinct features; for example, the ATP binding loop (residues 8–15) had several hydrogen bonds to water in both of the apo simulations, but very few in the SB simulations. Substrate binding and the associated solvent exclusion events were not studied in this work.

Long-lived residue-water hydrogen bonds (lifetime > 1 ns) observed in *t*0-closed simulations included Lys^{23}, Arg^{123}, Arg^{156}, Arg^{167}, Thr^{191}, Tyr^{171}, Tyr^{181}, and Lys^{195}, whereas in the *t*0-open simulations, long-lived residue-water hydrogen bonds were only observed for Arg^{167}. Therefore, the specific behaviors of residue-water hydrogen bonds did reflect the structures of AK, highlighting the fact that an explicit solvent model can provide such detailed information. However, we did not observe a discernible correlation between protein-water hydrogen bond occupancy and AK conformational changes.

CONCLUSIONS

In this work, we systematically examined the open-to-closed and closed-to-open transitions of AK by performing a series of all-atom MD simulations in explicit water. The effects of substrate binding and hinge unfolding on conformational changes were analyzed by starting MD simulations

from different initial structures and substrate-binding configurations. No bias potential was applied to perturb the protein dynamics. First, our results affirm the notion that there are at least two pathways connecting closed and open AK (Fig. 2), as previously suggested by x-ray crystallography and predicted by CG modeling. However, dynamic pathways obtained with atomic resolution and without the use of any bias potential have not yet been reported. All-atom MD simulations indicate that opening and partial closing transitions can be induced by substrate-mediated interactions. During conformational changes, tertiary contacts modulated by ATP and AMP and changes in local secondary structures (such as the overstretched α3 helix) both play significant roles in driving structural transitions. On the other hand, significant changes in the density and density fluctuations of surrounding water were not observed during the conformational changes of AK.

Although the apparent difference between the open and closed states of AK is in the distances between LID and NMP_{bind} and the CORE, the all-atom MD simulations provide direct evidence that the structure of a hinge motif that couples different domains can also affect the pathways of conformational change. The Pro^{177} hinge connects the CORE and LID of AK and is far away from the active site. We showed that when the Pro^{177} hinge is folded, the opening and closing transitions can be induced by substrate-mediated interactions. In the *t*0-closed–apo simulation, AK opened spontaneously in the absence of substrate-mediated interactions. Local unfolding of the Pro^{177} hinge, on the other hand, led to a more expanded active site and induced alternative interdomain interactions. The expanded active site and alternative tertiary contacts appear to prevent the opening of AK from a closed structure, even in the absence of substrate-mediated interactions. The local folding/unfolding of Pro^{177} hinge and the transition between the open and closed forms of AK are thus highly coupled. Local unfolding and the resulting changes in tertiary contacts could be exploited as a mechanism to modulate the conformational change and allostery of AK. This hypothesis can be tested by measuring the dynamics of AK conformational changes together with that of the local unfolding of the Pro^{177} hinge. According to this hypothesis, mutating Pro^{177} into residues with different stabilities in maintaining a helical structure is also expected to affect the equilibrium as well as the dynamics of conformational changes.

SUPPORTING MATERIAL

Twelve figures and references are available at http://www.biophysj.org/biophysj/supplemental/S0006-3495(10)01189-6.

We thank Dr. Yang-Wen Tang and Dr. Haw Yang for insightful discussions and helpful comments on the manuscript. Sixty percent of the research was performed using resources of the National Energy Research Scientific Computing Center, which is supported by the Office of Science of the U.S. Department of Energy under Contract No. DE-AC02-05CH11231. Forty percent of the research was performed using the Environmental Molecular Sciences Laboratory, a National Scientific User Facility sponsored by the Department of Energy's Office of Biological and Environmental Research and located at Pacific Northwest National Laboratory.

This research was supported by the American Chemical Society Petroleum Research Fund, ACS-PRF-49727-DNI6, and the College of Chemistry, University of California, Berkeley.

REFERENCES

1. Swain, J. F., and L. M. Gierasch. 2006. The changing landscape of protein allostery. *Curr. Opin. Struct. Biol.* 16:102–108.
2. Smock, R. G., and L. M. Gierasch. 2009. Sending signals dynamically. *Science.* 324:198–203.
3. Ringe, D., and G. A. Petsko. 2008. How enzymes work. *Science.* 320:1428–1429.
4. Bogoyevitch, M. A., and D. P. Fairlie. 2007. A new paradigm for protein kinase inhibition: blocking phosphorylation without directly targeting ATP binding. *Drug Discov. Today.* 12:622–633.
5. Remy, I., I. A. Wilson, and S. W. Michnick. 1999. Erythropoietin receptor activation by a ligand-induced conformation change. *Science.* 283:990–993.
6. Lee, G. M., and C. S. Craik. 2009. Trapping moving targets with small molecules. *Science.* 324:213–215.
7. Cui, Q., and M. Karplus. 2008. Allostery and cooperativity revisited. *Protein Sci.* 17:1295–1307.
8. Fischer, E. 1894. Einfluss der Configuration auf die Wirkung der Enzyme. *Ber. Dtsch. Chem. Ges.* 27:2985–2993.
9. Koshland, D. E. 1958. Application of a theory of enzyme specificity to protein synthesis. *Proc. Natl. Acad. Sci. USA.* 44:98–104.
10. Berger, C., S. Weber-Bornhauser, …, H. R. Bosshard. 1999. Antigen recognition by conformational selection. *FEBS Lett.* 450:149–153.
11. Bosshard, H. R. 2001. Molecular recognition by induced fit: how fit is the concept? *News Physiol. Sci.* 16:171–173.
12. Myong, S., B. C. Stevens, and T. Ha. 2006. Bridging conformational dynamics and function using single-molecule spectroscopy. *Structure.* 14:633–643.
13. Cui, Q., and M. Karplus. 2003. Catalysis and specificity in enzymes: a study of triosephosphate isomerase and comparison with methyl glyoxal synthase. *In* Protein Simulations. Academic Press, San Diego. 315–372.
14. Eppler, R. K., E. P. Hudson, …, D. S. Clark. 2008. Biocatalyst activity in nonaqueous environments correlates with centisecond-range protein motions. *Proc. Natl. Acad. Sci. USA.* 105:15672–15677.
15. Eppler, R. K., R. S. Komor, …, D. S. Clark. 2006. Water dynamics and salt-activation of enzymes in organic media: mechanistic implications revealed by NMR spectroscopy. *Proc. Natl. Acad. Sci. USA.* 103:5706–5710.
16. Wolf-Watz, M., V. Thai, …, D. Kern. 2004. Linkage between dynamics and catalysis in a thermophilic-mesophilic enzyme pair. *Nat. Struct. Mol. Biol.* 11:945–949.
17. Adén, J., and M. Wolf-Watz. 2007. NMR identification of transient complexes critical to adenylate kinase catalysis. *J. Am. Chem. Soc.* 129:14003–14012.
18. Gerstein, M., and W. Krebs. 1998. A database of macromolecular motions. *Nucleic Acids Res.* 26:4280–4290.
19. Karplus, M., and J. Kuriyan. 2005. Molecular dynamics and protein function. *Proc. Natl. Acad. Sci. USA.* 102:6679–6685.
20. Chu, J. W., and G. A. Voth. 2005. Allostery of actin filaments: molecular dynamics simulations and coarse-grained analysis. *Proc. Natl. Acad. Sci. USA.* 102:13111–13116.
21. Kim, P. S., and R. L. Baldwin. 1990. Intermediates in the folding reactions of small proteins. *Annu. Rev. Biochem.* 59:631–660.

22. Englander, J. J., C. Del Mar, …, V. L. Woods, Jr. 2003. Protein structure change studied by hydrogen-deuterium exchange, functional labeling, and mass spectrometry. *Proc. Natl. Acad. Sci. USA.* 100:7057–7062.

23. Englander, S. W. 2000. Protein folding intermediates and pathways studied by hydrogen exchange. *Annu. Rev. Biophys. Biomol. Struct.* 29:213–238.

24. Englander, S. W., J. J. Englander, …, S. J. Gill. 1992. Hydrogen exchange measurement of the free energy of structural and allosteric change in hemoglobin. *Science.* 256:1684–1687.

25. Fierz, B., A. Reiner, and T. Kiefhaber. 2009. Local conformational dynamics in α-helices measured by fast triplet transfer. *Proc. Natl. Acad. Sci. USA.* 106:1057–1062.

26. Panchal, S. C., N. S. Bhavesh, and R. V. Hosur. 2001. Real time NMR monitoring of local unfolding of HIV-1 protease tethered dimer driven by autolysis. *FEBS Lett.* 497:59–64.

27. Dürrschmidt, P., J. Mansfeld, and R. Ulbrich-Hofmann. 2005. An engineered disulfide bridge mimics the effect of calcium to protect neutral protease against local unfolding. *FEBS J.* 272:1523–1534.

28. Shaw, B. F., A. Durazo, …, J. S. Valentine. 2006. Local unfolding in a destabilized, pathogenic variant of superoxide dismutase 1 observed with H/D exchange and mass spectrometry. *J. Biol. Chem.* 281:18167–18176.

29. Whitten, S. T., B. García-Moreno E, and V. J. Hilser. 2005. Local conformational fluctuations can modulate the coupling between proton binding and global structural transitions in proteins. *Proc. Natl. Acad. Sci. USA.* 102:4282–4287.

30. Schrank, T. P., D. W. Bolen, and V. J. Hilser. 2009. Rational modulation of conformational fluctuations in adenylate kinase reveals a local unfolding mechanism for allostery and functional adaptation in proteins. *Proc. Natl. Acad. Sci. USA.* 106:16984–16989.

31. Vertrees, J., P. Barritt, …, V. J. Hilser. 2005. COREX/BEST server: a web browser-based program that calculates regional stability variations within protein structures. *Bioinformatics.* 21:3318–3319.

32. Miyashita, O., J. N. Onuchic, and P. G. Wolynes. 2003. Nonlinear elasticity, proteinquakes, and the energy landscapes of functional transitions in proteins. *Proc. Natl. Acad. Sci. USA.* 100:12570–12575.

33. Hyeon, C., P. A. Jennings, …, J. N. Onuchic. 2009. Ligand-induced global transitions in the catalytic domain of protein kinase A. *Proc. Natl. Acad. Sci. USA.* 106:3023–3028.

34. Whitford, P. C., O. Miyashita, …, J. N. Onuchic. 2007. Conformational transitions of adenylate kinase: switching by cracking. *J. Mol. Biol.* 366:1661–1671.

35. Müller, C. W., G. J. Schlauderer, …, G. E. Schulz. 1996. Adenylate kinase motions during catalysis: an energetic counterweight balancing substrate binding. *Structure.* 4:147–156.

36. Müller, C. W., and G. E. Schulz. 1992. Structure of the complex between adenylate kinase from *Escherichia coli* and the inhibitor Ap5A refined at 1.9 A resolution. A model for a catalytic transition state. *J. Mol. Biol.* 224:159–177.

37. Noda, L. 1973. Adenylate kinase. *In* The Enzymes. P. D. Boyer, editor. Academic Press, New York. 279–305.

38. Maragakis, P., and M. Karplus. 2005. Large amplitude conformational change in proteins explored with a plastic network model: adenylate kinase. *J. Mol. Biol.* 352:807–822.

39. Lou, H. F., and R. I. Cukier. 2006. Molecular dynamics of apo-adenylate kinase: a distance replica exchange method for the free energy of conformational fluctuations. *J. Phys. Chem. B.* 110:24121–24137.

40. Arora, K., and C. L. Brooks, 3rd. 2007. Large-scale allosteric conformational transitions of adenylate kinase appear to involve a population-shift mechanism. *Proc. Natl. Acad. Sci. USA.* 104:18496–18501.

41. Hanson, J. A., K. Duderstadt, …, H. Yang. 2007. Illuminating the mechanistic roles of enzyme conformational dynamics. *Proc. Natl. Acad. Sci. USA.* 104:18055–18060.

42. Tan, Y. W., J. A. Hanson, and H. Yang. 2009. Direct Mg(2+) binding activates adenylate kinase from *Escherichia coli*. *J. Biol. Chem.* 284:3306–3313.

43. Sheng, X. R., X. Li, and X. M. Pan. 1999. An iso-random Bi Bi mechanism for adenylate kinase. *J. Biol. Chem.* 274:22238–22242.

44. Berry, M. B., E. Y. Bae, …, G. N. Phillips. 2006. Crystal structure of ADP/AMP complex of *Escherichia coli* adenylate kinase. *Proteins.* 62:555–556.

45. Shapiro, Y. E., E. Kahana, …, E. Meirovitch. 2002. Domain flexibility in ligand-free and inhibitor-bound *Escherichia coli* adenylate kinase based on a mode-coupling analysis of 15N spin relaxation. *Biochemistry.* 41:6271–6281.

46. Shapiro, Y. E., M. A. Sinev, …, E. Meirovitch. 2000. Backbone dynamics of *Escherichia coli* adenylate kinase at the extreme stages of the catalytic cycle studied by (15)N NMR relaxation. *Biochemistry.* 39:6634–6644.

47. Henzler-Wildman, K. A., V. Thai, …, D. Kern. 2007. Intrinsic motions along an enzymatic reaction trajectory. *Nature.* 450:838–844.

48. Daily, M. D., G. N. Phillips, Jr., and Q. A. Cui. 2010. Many local motions cooperate to produce the adenylate kinase conformational transition. *J. Mol. Biol.* 400:618–631.

49. Kern, P., R. M. Brunne, and G. Folkers. 1994. Nucleotide-binding properties of adenylate kinase from *Escherichia coli*: a molecular dynamics study in aqueous and vacuum environments. *J. Comput. Aided Mol. Des.* 8:367–388.

50. Kubitzki, M. B., and B. L. de Groot. 2008. The atomistic mechanism of conformational transition in adenylate kinase: a TEE-REX molecular dynamics study. *Structure.* 16:1175–1182.

51. Pontiggia, F., A. Zen, and C. Micheletti. 2008. Small- and large-scale conformational changes of adenylate kinase: a molecular dynamics study of the subdomain motion and mechanics. *Biophys. J.* 95:5901–5912.

52. Krishnamurthy, H., H. F. Lou, …, R. I. Cukier. 2005. Associative mechanism for phosphoryl transfer: a molecular dynamics simulation of *Escherichia coli* adenylate kinase complexed with its substrates. *Proteins.* 58:88–100.

53. Snow, C., G. Y. Qi, and S. Hayward. 2007. Essential dynamics sampling study of adenylate kinase: comparison to citrate synthase and implication for the hinge and shear mechanisms of domain motions. *Proteins.* 67:325–337.

54. Henzler-Wildman, K. A., M. Lei, …, D. Kern. 2007. A hierarchy of timescales in protein dynamics is linked to enzyme catalysis. *Nature.* 450:913–916.

55. Beckstein, O., E. J. Denning, …, T. B. Woolf. 2009. Zipping and unzipping of adenylate kinase: atomistic insights into the ensemble of open<—>closed transitions. *J. Mol. Biol.* 394:160–176.

56. Diederichs, K., and G. E. Schulz. 1991. The refined structure of the complex between adenylate kinase from beef heart mitochondrial matrix and its substrate AMP at 1.85 A resolution. *J. Mol. Biol.* 217:541–549.

57. Schlauderer, G. J., K. Proba, and G. E. Schulz. 1996. Structure of a mutant adenylate kinase ligated with an ATP-analogue showing domain closure over ATP. *J. Mol. Biol.* 256:223–227.

58. Chu, J. W., and G. A. Voth. 2007. Coarse-grained free energy functions for studying protein conformational changes: a double-well network model. *Biophys. J.* 93:3860–3871.

59. Lu, Q., and J. Wang. 2008. Single molecule conformational dynamics of adenylate kinase: energy landscape, structural correlations, and transition state ensembles. *J. Am. Chem. Soc.* 130:4772–4783.

60. Whitford, P. C., J. K. Noel, …, J. N. Onuchic. 2009. An all-atom structure-based potential for proteins: bridging minimal models with all-atom empirical forcefields. *Proteins.* 75:430–441.

61. Bratko, D., R. A. Curtis, …, J. M. Prausnitz. 2001. Interaction between hydrophobic surfaces with metastable intervening liquid. *J. Chem. Phys.* 115:3873–3877.

62. Giovambattista, N., C. F. Lopez, …, P. G. Debenedetti. 2008. Hydrophobicity of protein surfaces: separating geometry from chemistry. *Proc. Natl. Acad. Sci. USA.* 105:2274–2279.

63. Willard, A. P., and D. Chandler. 2009. Coarse-grained modeling of the interface between water and heterogeneous surfaces. *Faraday Discuss.* 141:209–220, discussion 309–346.

64. Godawat, R., S. N. Jamadagni, and S. Garde. 2009. Characterizing hydrophobicity of interfaces by using cavity formation, solute binding, and water correlations. *Proc. Natl. Acad. Sci. USA.* 106:15119–15124.

65. MacKerell, A. D., D. Bashford, …, M. Karplus. 1998. All-atom empirical potential for molecular modeling and dynamics studies of proteins. *J. Phys. Chem. B.* 102:3586–3616.

66. Mackerell, Jr., A. D., M. Feig, and C. L. Brooks, 3rd. 2004. Extending the treatment of backbone energetics in protein force fields: limitations of gas-phase quantum mechanics in reproducing protein conformational distributions in molecular dynamics simulations. *J. Comput. Chem.* 25:1400–1415.

67. Bellinzoni, M., A. Haouz, …, P. M. Alzari. 2006. The crystal structure of *Mycobacterium tuberculosis* adenylate kinase in complex with two molecules of ADP and Mg^{2+} supports an associative mechanism for phosphoryl transfer. *Protein Sci.* 15:1489–1493.

68. Deville, J., J. Rey, and M. Chabbert. 2008. Comprehensive analysis of the helix-X-helix motif in soluble proteins. *Proteins.* 72:115–135.

69. ten Wolde, P. R., and D. Chandler. 2002. Drying-induced hydrophobic polymer collapse. *Proc. Natl. Acad. Sci. USA.* 99:6539–6543.

70. Zhou, R., X. Huang, …, B. J. Berne. 2004. Hydrophobic collapse in multidomain protein folding. *Science.* 305:1605–1609.

71. Miller, 3rd, T. F., E. Vanden-Eijnden, and D. Chandler. 2007. Solvent coarse-graining and the string method applied to the hydrophobic collapse of a hydrated chain. *Proc. Natl. Acad. Sci. USA.* 104:14559–14564.

72. Sarupria, S., and S. Garde. 2009. Quantifying water density fluctuations and compressibility of hydration shells of hydrophobic solutes and proteins. *Phys. Rev. Lett.* 103:037803.

73. Willard, A. P., and D. Chandler. 2008. The role of solvent fluctuations in hydrophobic assembly. *J. Phys. Chem. B.* 112:6187–6192.